Supplementary Text

Direction Selectivity

Figure S1B-H reports no evidence for directional selectivity when stimulating pairs of individual inputs to the LGMD. Putative direction selective responses presynaptic to the LGMD have been documented in an earlier report [13], by imaging intracellular calcium transients in the LGMD elicited by the motion of black bars in its receptive field. The current results suggest that this direction selectivity arises through mechanisms operating on a larger spatial scale than the one tested here.

Photoreceptor Transients

The difference in photoreceptor transients elicited by translating edges (Fig. 2B) and luminance changes that target individual facets (Fig. 2C) is likely due to two main differences between visual stimulation using a CRT and that using a DLP projector in conjunction with microscope optics and water immersion of the eye. First, the microscope has a much larger overall brightness than the CRT and thus both its black and white levels are brighter than those of the CRT. As a consequence, the microscope is more likely to engage non-linear transduction mechanisms in photoreceptors. This is illustrated in Figure S2A, where we show that the photoreceptor transients are much reduced when an aperture is closed in a non-image plane of the light projection path to decrease the overall light intensity.

A second difference is that during microscopic stimulation the photoreceptor is kept at the stimulus' minimum brightness, then the stimulus is transitioned to bright and finally back to dark. This last part of the response (OFF) is what we observe. The situation is quite different during edge stimulation experiments since the CRT is kept bright except when a dark edge passes through. Therefore, the photoreceptor is not in the same adaptation state in the two experiments. In Figure S2B we show that if the CRT is kept black (2 cd/m^2), and turned bright only 100 ms before presenting the black edge, the photoreceptor OFF response produces non-linear transients resembling those observed with the DLP.

In summary, our experimental data suggest that the difference in response is caused by the amount of light generated by the two apparatuses and differences in photoreceptor adaptation level. However, those differences have no impact on our conclusions as shown in Fig. 3 and 4.

The main determinant of the effect we observe is the slope of the photoreceptor response that is very similar under both stimulation conditions (Fig. 2D).

Supplementary Figure Legends

Supplementary Figure 1 - Custom microscope for visual stimulation of single ommatidia and testing the direction selectivity of LGMD responses to apparent motion (related to Figure 1). A Optical diagram of the microscope light path. The stimulus is generated using a Digital Light Projection (DLP) projector, whose image is focused onto the image plane (IM) of the compound microscope. A beamsplitter arrangement allows for registration of the eye and the stimulus, half of which reflects off the beamsplitter/mirror while the other half projects onto the eye, since the camera simultaneously views the image plane and the mirror plane. The stimulus projection path shares an image plane with the microscopic image path (IM), ensuring that the relative positions and sizes of stimulus image and microscopic image are preserved in the front focal plane of the objective, the specimen plane. Black labels denote parts. Gray labels show important distances in the optical path. Objective = Olympus 20x/0.5 NA WI or 10x/0.3NA WI, L1 = f100 achromat, L2/L3 = f75 achromat, L4 = f50 achromat, Projector Objective = 35mm integrated lens, BS = 50/50 AR-coated plate beamsplitter, Mirrors = plane, first-surface mirrors. Inset is a sample image taken with the microscope of a locust eye under water immersion. The middle of the field is focused past the surface of the eye, behind the ommatidial lenses, while the edges of the field are focused on the lens surfaces. Ommatidia selected for visual stimulation in experiments were in similar planes of focus as those in the center of the field. **B** LGMD membrane potential traces from a single direction selectivity experiment. A pair of facets were targeted for stimulation with the microscope. Panel ***i*** shows the responses (mean median-filtered membrane potential and SEM envelope) to simultaneous stimulation of the two facets (green) and the responses to stimulation of each facet alone (black, solid and dashed). The top traces show the stimulus for each facet. Panels ***ii*** and ***iii*** show the responses at the two non-zero ISIs tested. Blue stimuli/responses show conditions where the arbitrarily chosen first facet leads the second, while red designates where the second leads the first. **C** Summation indices (SI) of responses as a function of ISI value for the experiment shown in A. A direction selectivity index (DSI) was calculated for the two non-zero delays as $DSI = (SI_{1lead} - SI_{1lag}) / (SI_{1lead} + SI_{1lag})$. Its

value is given next to the corresponding delays. Symbols and error bars show mean and SEM of the summation indices, and the color of the plot shading corresponds with trace coloring in B. Single facet response SIs are plotted, each slightly offset from 0, as unconnected symbols. Only OFF responses are shown. **D** Summation indices for the population of facet pairs stimulated (6 animals, 24 facet pairs). Since apparent motion responses were probed using facet pairs of different orientations, experiments are pooled such that positive ISIs correspond to motion in the anterior to posterior or dorsal to ventral directions (blue), and opposite directions are negative (red). Both ON (circles) and OFF (x's) are shown as population mean and SEM. **E** Histogram of the distribution of DSI values obtained in all experimental conditions (4 per facet pair; ON or OFF and 2 ISIs). The median DSI value (0.011) is not significantly different from zero (Wilcoxon signed-rank, n=96, $p>0.07$). **F, G, H** DSI histograms broken down by stimulus polarity, ISI, and apparent motion orientation. No partitioning of the data yielded populations of DSIs that were significantly different from each other (Wilcoxon rank-sum, $p>0.07$, 0.22, 0.94 for polarity, ISI, and orientation).

Supplementary Figure 2 - Modulating the strength of photoreceptor transients (related to Figure 2). A Shows the OFF responses of a single representative photoreceptor under microscope-delivered single facet stimulation. Top traces show the stimulus command luminance over time. Solid traces below show the responses to the stimulus when the luminance is bright. Dashed traces show the responses when an aperture was partially closed in a non-image plane of the projection path to decrease the overall luminance. The resting V_m is defined as the membrane potential during the final 200ms of the intertrial interval. The average resting V_m was -40 mV with a average drop of 7.5 mV after narrowing the aperture. Notice that the response transients are much larger when the luminance was high. **B** Shows the responses to dark edges presented on a CRT monitor. Top traces show edge position over time. Middle traces show photoreceptor responses when the monitor was bright (90 cd/m^2) during the intertrial interval (5 sec). The bottom traces show the responses of the same receptor when the monitor was dark during the intertrial interval (2 cd/m^2) and turned bright 100 ms before edge motion began. The average resting V_m when the monitor was dark was -54 mV.

Supplementary Figure 3 - Mean LGMD responses to conventional (normal), coarse, and constant-rate looming stimuli (related to Figure 4). A Mean LGMD firing rates averaged across trials in all experiments, without normalization. Formatting follows Figure 4A with the omission of spike rasters and the addition of black traces showing the responses to normal looming stimuli (mean and SEM envelope; normal looming: n=115-118 trials in 12 animals; coarse and constant-rate data is the same as in Figure 4). **B, C** Distributions of peak firing rates and spike counts for normal (grey), coarse (dark color), and constant-rate (light color) looming stimuli. Formatting again follows Fig. 4. Coarse and constant-rate looming data are replotted for comparison with normal looming responses. **C** Distributions of spike counts during a 500 ms window around the peak of the normal looming response in each experiment, indicated by the gray shaded regions in panel A. **D** Timing of the peak firing rate as a function of $l/|v|$ for normal looming (black), coarse looming (red), and constant-rate looming (light red) stimuli. Circles are population mean times, with error bars indicating SEM. Dashed lines show linear, least-squares fits to the data. The fit to normal looming stimuli gave slope and intercept values of 4.4 and -18.7 ms, respectively (see Figure 4D for others). The fitted slope corresponds to an angular threshold value of 25.7°.

Supplementary Figure 4 - Details of pseudo-looming and coarse/constant rate looming stimuli (related to Figures 3 and 4). A Luminance change durations used to stimulate single facets in pseudo-looming experiments, plotted as a function of their respective onset time for each of the 15 facet rows (0 is luminance change onset time for the first row). Slow, medium, and fast sequences are shown in blue, red and green, respectively. Open circles (light colors) show the same luminance change durations after a representative shuffle. **B** Normalized illuminance over the 15 facet rows during the three pseudo-looming stimuli, plotted as a function of the onset time of the first luminance change. To compare pseudo-looming and looming stimuli – even though there are substantial differences between them – we fitted these normalized illuminance changes with those generated by looming stimuli integrated over a 45° section of visual space. A 45º section was selected since it matches that covered by 15 facet rows, assuming that individual facets span 3° with non-overlapping receptive fields. The fits were carried out on the accelerating portion of the normalized illuminance curves, from the onset time of the first luminance change (0 s) to the completion of the luminance change in the last row (266 ms later,

marked by the black vertical line). The subsequent decelerating part of the curves corresponds to (initial) slower changes that proceed after the last facet row changes are completed. This portion of pseudo-looming stimuli does not have an equivalent in looming stimuli. **C** Fits of the normalized illuminance resulting from looming stimuli (black lines) to those of the pseudo-looming stimuli. Each pseudo-loom illuminance trace (**C**) was normalized so that it varied between 0 and 1 in the 0-266 ms time period. Looming stimulus fits were allowed to vary over three parameters: $l/|v|$, time period during the loom, and the position of the 45º window, relative to the center of the looming stimulus. Resulting $l/|v|$ values were 105, 46, and 15 ms for slow, medium, and fast pseudo-looming stimuli, respectively. **D** Individual 3ºx3º "pixel" brightnesses during coarse and constant rate looming stimuli ($l/|v|$ = 40ms). While the luminance changes occurring later in the coarse looming stimulus are more rapid those that occur earlier, luminance changes at all pixels in the constant rate loom occur at the same rate. The angular size of the corresponding normal looming stimulus is shown above for reference. **E** Comparison of coarse/constant rate looming stimuli with normal ones. Each trace shows the percentage deviation in total screen brightness from that of a normal looming stimulus throughout the time course of the stimulus. Negative values mean that the coarse/constant rate looming stimulus is darker than a normal loom (simulating the approach of a black square), positive values mean that the modified loom is brighter. Coarse looming stimuli are shown in the dark colors, while constant-rate stimuli are plotted in light colors with dashed lines. Mean, frame-wise deviations are 0.05% for coarse looming stimuli and are in the range of 0.17-0.24% for constant rate stimuli.

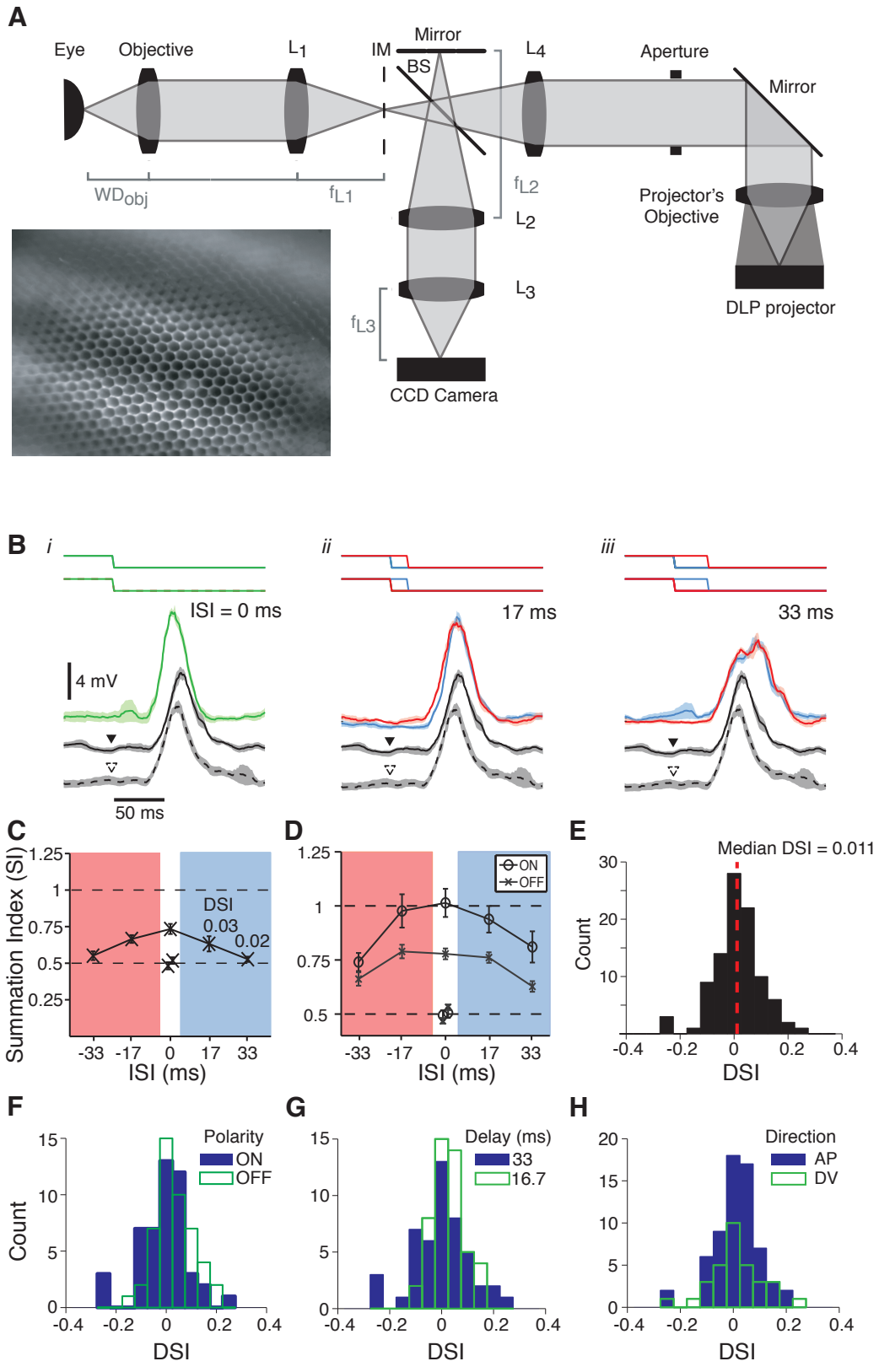

Jones and Gabbiani, Figure S1

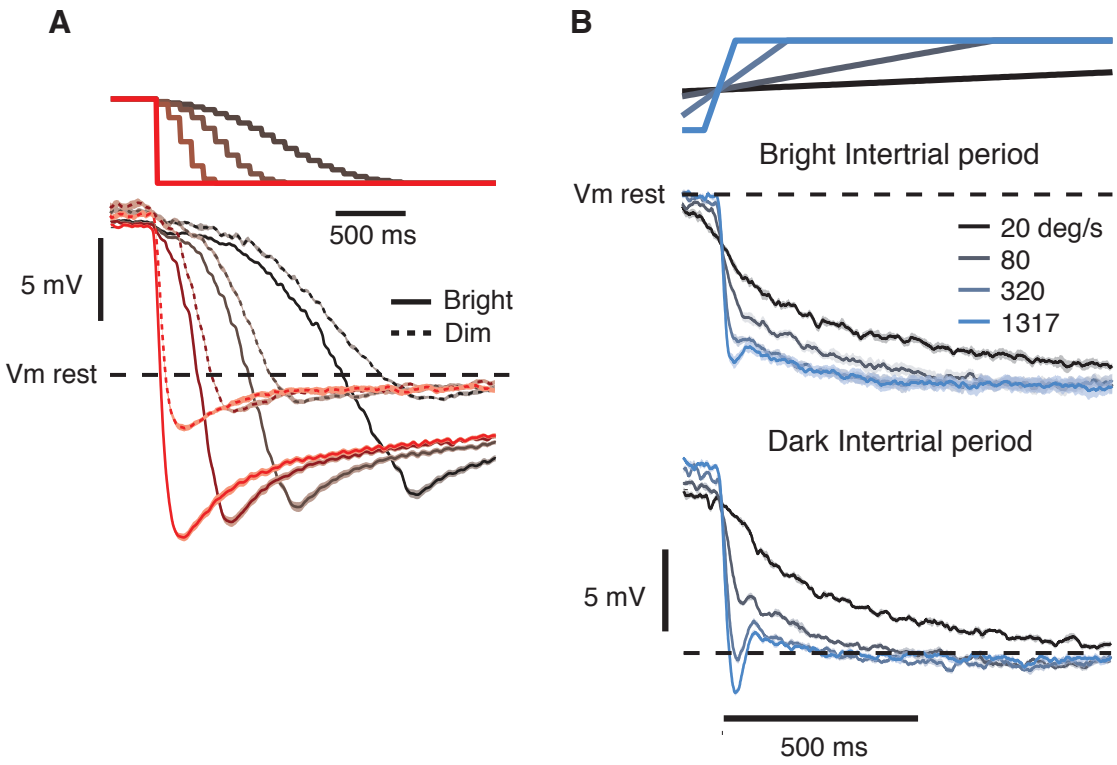

Jones and Gabbiani, Figure S2

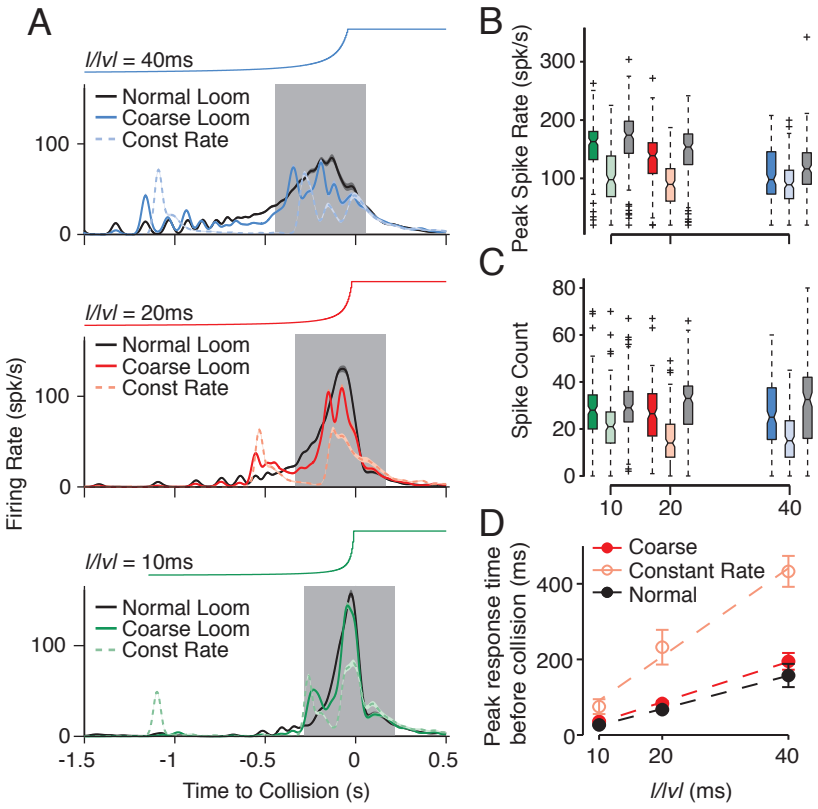

Jones and Gabbiani, Figure S3

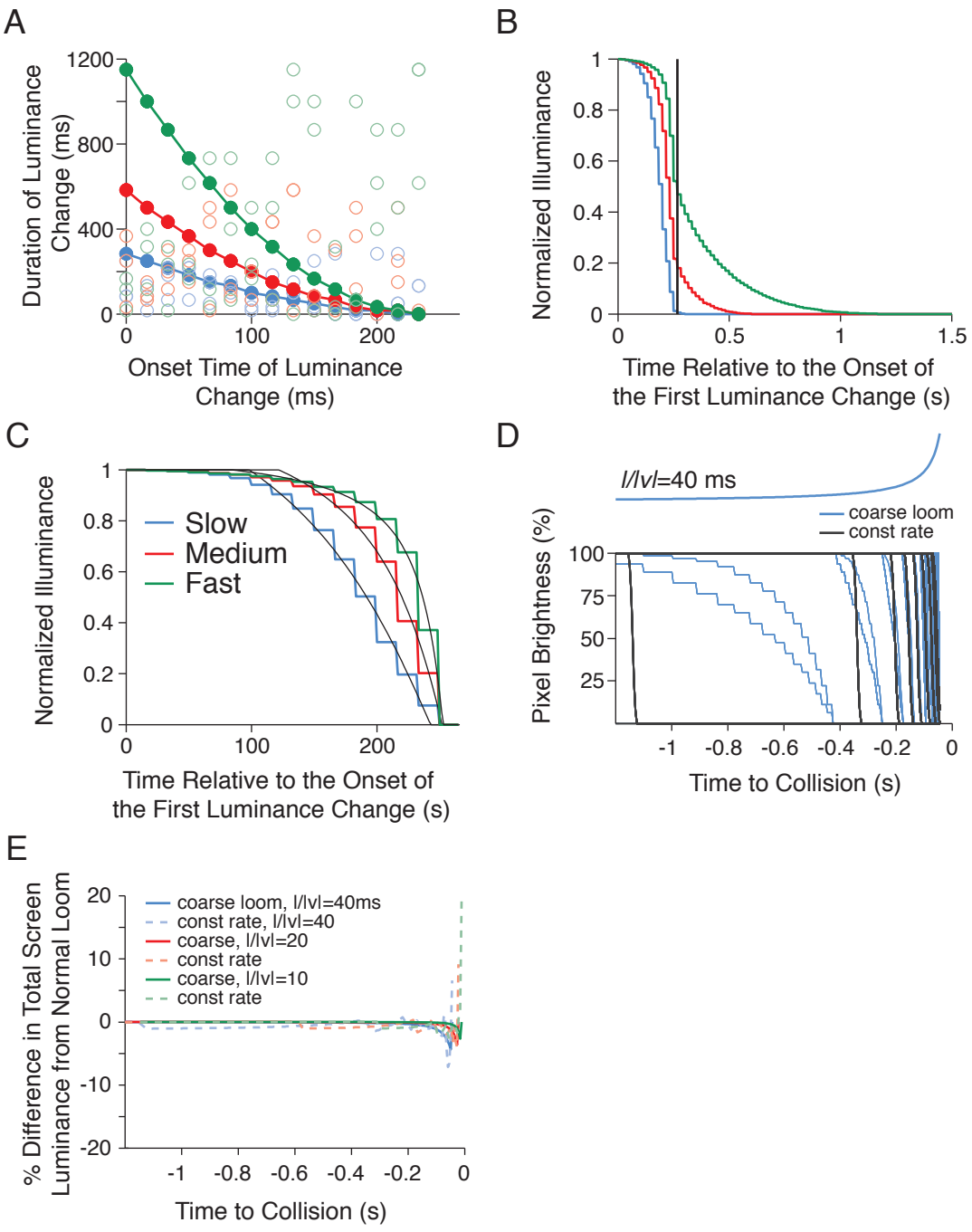

Jones and Gabbiani, Figure S4